International Journal of Minerals, Metallurgy and Materials
Volume 28, Number 9, September 2021, Page 1429
https://doi.org/10.1007/s12613-020-2181-2

Fractal and microscopic quantitative characterization of unclassified tailings flocs

Di Zheng[1,2], *Wei-dong Song*[1,2], *Yu-ye Tan*[1,2], *Shuai Cao*[1,2], *Zi-long Yang*[1,2], *and Li-juan Sun*[1,2,3]

1) State Key Laboratory of High-Efficient Mining and Safety of Metal Mines of Ministry of Education, University of Science and Technology Beijing, Beijing 100083, China

2) School of Civil and Resources Engineering, University of Science and Technology Beijing, Beijing 100083, China

3) State Key Laboratory for Nonlinear Mechanics (LNM) Institute of Mechanics, Chinese Academy of Science, Beijing 100190, China

(Received: 28 June 2020; revised: 14 August 2020; accepted: 31 August 2020)

Abstract: A series of laboratory investigations are conducted to analyze the effect of flocculant type on the spatial morphology and microstructural characteristics of flocs during the flocculation and settling of tailings. Four flocculant types (i.e., ZYZ, JYC-2, ZYD, and JYC-1) are considered in this study. The fractal characteristics and internal structures of tailings flocs with different flocculant types and settlement heights are analyzed by conducting scanning electron microscopy and X-ray micro-computed tomography scanning experiments based on the fractal theory. Results show that unclassified tailings flocs are irregular clusters with fractal characteristics, and the flocculation effect of the four flocculant types has the following trend: ZYZ > JYC-2 > ZYD > JYC-1. The size and average grayscale value of tailings flocs decrease with the increase in settlement height. The average grayscale values at the top and bottom are 144 and 103, respectively. The settlement height remarkably affects the pore distribution pattern, as reflected in the constructed three-dimensional pore model of tailings flocs. The top part of flocs has relatively good penetration, whereas the bottom part of flocs has mostly dispersed pores. The number of pores increases exponentially with the increase in settlement height. By contrast, the size of pores initially increases and subsequently decreases with the increase in settlement height.

Keywords: tailings flocs; fractal dimension; settlement height; grayscale value; three-dimensional pore model

1. Introduction

The filling mining method has been widely used in various mines because of the increase in people's environmental awareness [1–4]. Flocculation and settling technologies for tailings filling slurry in mines are important [5–7]. Flocculants are added to a dispersed tailings solution to cause tailings particles in water to aggregate into large tailings flocs through charge adsorption and consequently induce bridging and cross-linking [8–12], which further cause the tailings to aggregate into large tailings flocs, thereby improving the particle settling rate [13–17].

The mechanisms of action of flocculation and settling have been the focus of numerous studies. Eswaraiah *et al.* [18] showed that sedimentation speed is repeatedly improved by flocculants. Anionic flocculants are more effective than cationic and neutral flocculants in increasing the settling speed of slurries. Wu *et al.* [19] determined that the relative flocculation rate initially increases and subsequently decreases with the increase in pH, flocculant unit consumption, and shear rate; conversely, the relative flocculation rate gradually decreases with the increase in solid volume fraction of the slurry. Researchers [20–21] demonstrated that settling velocity is negatively correlated with feed concentration at a certain unit consumption, whereas limit concentration is positively correlated with feed concentration. Dwari *et al.* [22] observed that the ionicity and molecular weight of the flocculants have a significant effect on the tailings settling properties. Bian *et al.* [23] investigated the dynamic flocculation settlement of unclassified tailings and showed that sedimentation speed is positively correlated with the flocculant unit consumption, feeding speed, and mass fraction of the slurry.

Flocculated flocs are characterized by complex structures with different sizes, shapes, and voidages [24]. Fractal dimension is an important parameter used to measure flocs [25–27]. Liu *et al.* [28] observed that the fractal dimension of flocs formed by coal particles with small particle sizes is large, and these flocs are compact. Niu *et al.* [29] showed that the average particle size of flocs is positively related to their

Corresponding author: Yu-ye Tan E-mail: tanyuye@ustb.edu.cn

fractal dimension. Flocs formed with waxy corn starch have a large fractal dimension, dense structure, fast settling speed, and good flocculation effect. Xu and Dong [30] determined that the fractal dimension of flocs is distributed in a certain range, not a single value, under high shear conditions. Jiao *et al.* [31] showed that pore structures have obvious fractal characteristics, and the dimension of the pore box at the bottom of the bed is relatively small. As the bed height increases, the fractal dimension gradually increases.

X-ray micro-computed tomography (μCT) has been developed and widely used in the mining industry. X-ray computed tomography (CT) with nondestructive imaging is used to detect the internal structure of materials and reconstruct high-resolution images [32]. The complex geometry and internal texture of the material are characterized and analyzed by X-ray μCT [33]. Wang *et al.* [34] developed a feature-based segmentation algorithm and provided an accurate CT image processing method for microstructural analysis. Other scholars also used scanning electron microscopy (SEM) to examine the microstructure of flocs. Sharma *et al.* [35] analyzed the microstructure of flocs using cryo-SEM and observed the stabilization of kaolinite microflocs in the web formed by polymer chains. Zhang *et al.* [36] determined that the flocs formed by PTC1.0 had the best filtration property and were compact using SEM analysis.

Scholars all around the world have conducted considerable research on flocculation and settling but relatively few studies of the microstructure of flocs. In this study, the microstructure of unclassified tailings flocs is examined through experimental methods, such as SEM and μCT scanning, and the spatial morphology characteristics of flocs are analyzed based on the fractal theory to evaluate the effects of flocculation settlement of different flocculant types. The tailings floc in the best flocculant is selected, and its spatial morphology characteristics, grayscale characteristics, and pore structures are assessed to characterize the structure of the entire tailings floc in the microscale and provide a scientific basis for the selection of the appropriate flocculant. To provide intentional reference values for research on unclassified tailings flocs, the relationship between the settlement height and the quantity and size of pores was also analyzed from the microscopic point of view.

2. Experimental

2.1. Materials

The tested gold tailings used in this study are from a Shandong (China) gold mine. The tailings are manually sieved and scanned with a laser particle size analyzer to determine their particle size distribution, as shown in Fig. 1. The particle size distribution of the tailings indicates that approximately 62vol% of fine particles have tailings of less than 38 μm and approximately 51vol% of fine particles have tailings of less than 20 μm.

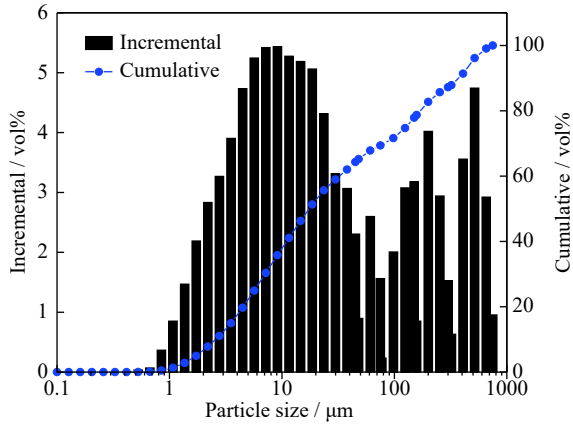

Fig. 1. Particle size distribution curve of the tailings.

The tailings density is 2.65 g/cm^3. Energy-dispersive spectroscopy point analysis is performed to analyze the chemical characteristics of the tailings, and the distribution map of each element is obtained, as shown in Fig. 2. The results show that the phase composition of the tailings sand is relatively simple, that is, mainly composed of quartz and mica. These two substances cannot be easily dissolved in water and dissociated into a single substance. Moreover, these two substances slightly affect the fluidity of the tailings filling slurry and the strength of the filling body. In contrast to the concentration distribution of the main elements, the concentration distribution of calcium and iron is low, indicating that the tailings contain calcium and iron inclusions.

Four flocculant types, that is, ZYZ, ZYD, JYC-1, and JYC-2, are mainly used in the experiment. Their basic properties are listed in Table 1. All of them are anionic flocculants mainly composed of polyacrylamide, with the molecular formula of $(C_3H_5NO)_n$. The main chain of polyacrylamide contains a large number of amide groups. The four flocculant types have similar chemical compositions but different production qualities, which result in different performance levels.

2.2. Experimental plan

Unclassified tailings are dispersed in a solution with a mass concentration of 15wt% and poured into a 1 L measuring cylinder. Then, 0.1wt% flocculant solution is prepared and added dropwise to the measuring cylinder using a dropper. The single consumption of the flocculant is 15 g/t. The slurry is fully mixed in the measuring cylinder using a stirrer. The stirrer is removed, and the mixture is left to stand for 10 min. Afterward, the floc is gently extracted with a long pipette [37], placed dropwise on a cut filter paper, and dried naturally for 24 h to prepare a sample for SEM. The four flocculant types were used to prepare the solution, and the experimental samples were obtained according to the previously presented steps. Fig. 3 shows the schematic diagram of the sampling location.

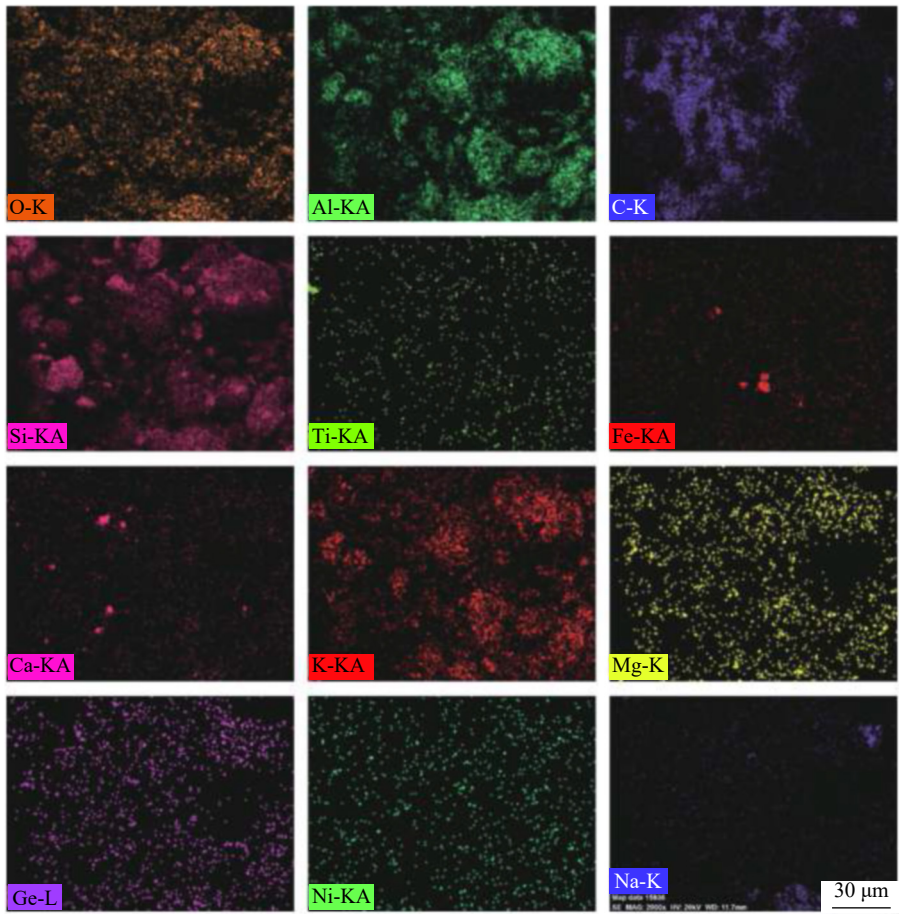

Fig. 2. Distribution of each element in the tailings.

Table 1. Basic properties of the flocculants

Flocculant	Solid content / wt%	Molecular weight / (10^6 u)	Charge density / wt%	Soluble in water
ZYZ	≥90	16–18	20–30	Yes
ZYD	≥88	16–18	22.5–27.5	Yes
JYC-1	≥88	16	20–30	Yes
JYC-2	≥90	18	22.5–27.5	Yes

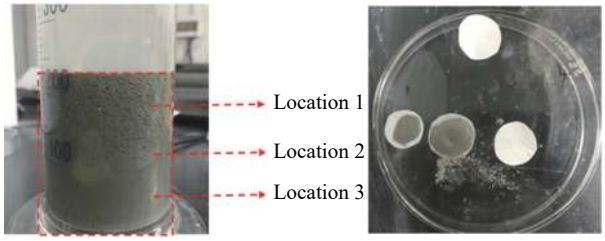

Fig. 3. Schematic of sampling using an electron microscope.

This procedure is repeated to prepare a sample for X-ray three-dimensional scanning by rapidly freezing the sample with liquid nitrogen and processing with a freeze dryer.

2.3. Experimental equipment

Carl Zeiss' tungsten filament SEM EVO 18 (as shown in Fig. 4) is used in the experiment, with an image size of 1000 × 750 px and an acceleration voltage of 20 kV. Before the test is performed, the samples are sprayed with carbon and held in place with conductive adhesive. After the samples are placed in a vacuum chamber for evacuation, SEM is conducted to analyze the microstructure of each sample at different magnifications.

A Nano Voxel 3502E model high-resolution X-ray (μCT) three-dimensional scanning imaging system (as shown in Fig. 5) is utilized in the X-ray three-dimensional scanning experiment, with a scanning resolution of 10 μm.

3. Results and discussion

3.1. Fractal theory characteristic of the flocculant SEM images

JYC-1, JYC-2, ZYZ, and ZYD are examined through

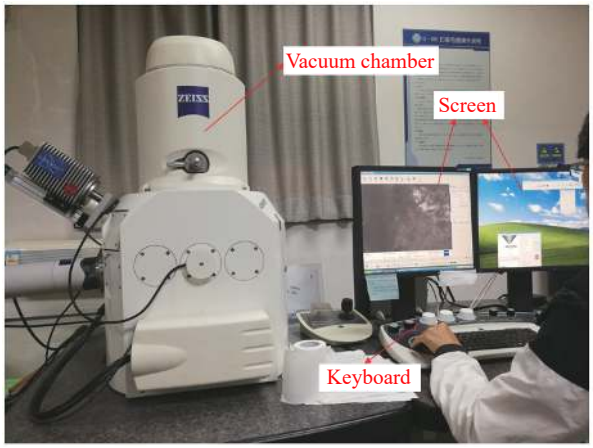

Fig. 4. Carl Zeiss' tungsten filament SEM EVO 18 used in the experiment.

SEM at 5000× magnification (Fig. 6). Black denotes pores, and other colors denote the floc and its structure.

Fractal geometry is a kind of geometry characterized by self-similarity, that is, irregular, fractured, or fragmented appearance. Scholars have conducted considerable research on aggregates formed by flocculation at high shear rates [38–40]. In this study, the flocs are not sheared to control for a single variable, which is a good approach to compare the effects of flocculants. Therefore, the fractal box dimension is used to characterize the fractal characteristics of flocs. N (N = 1, 2, 3, …) squares with side length r are taken to divide the image. The divided areas do not coincide, and the area containing the flocs is recorded as $N(r)$. Therefore, Eq. (1) is derived as follows:

$$N(r) = 1/r^D \tag{1}$$

Eq. (2) is derived after the logarithm is obtained, as follows:

Fig. 5. High-resolution X-ray three-dimensional scanning imaging system.

$$D = \frac{\lg N(r)}{-\lg r} \tag{2}$$

where D is the fractal dimension.

In SEM-based quantitative analysis, image binarization is important because it is the basis for conducting fractal analysis. Binarization, also known as threshold segmentation, is the process of setting the pixels of an image to 0 or 255, presenting the entire image with a clear black and white effect, and classifying each pixel. If $M \times N$ is the SEM image and $f(x, y)$ is the pixel grayscale value at the position of line (x − 1) and row (y − 1) in the image, where $0 \le x \le M$, $0 \le y \le$ N, $x, y \in$ integral number, then the principle of grayscale image binarization can be expressed as follows [41]:

$$f(x,y) = \begin{cases} 1, f(x,y) \ge T \\ 0, \text{else} \end{cases} \tag{3}$$

where T is the threshold. After binarization, all of the pixels of the image are only black and white. Binarization reduces the amount of data in an image; thus, the target object can be prominently outlined (Fig. 7). The binary images shown in Fig. 7 are obtained after the SEM images shown in Fig. 6 are binarized.

Fractal analysis is performed on the binary images of the

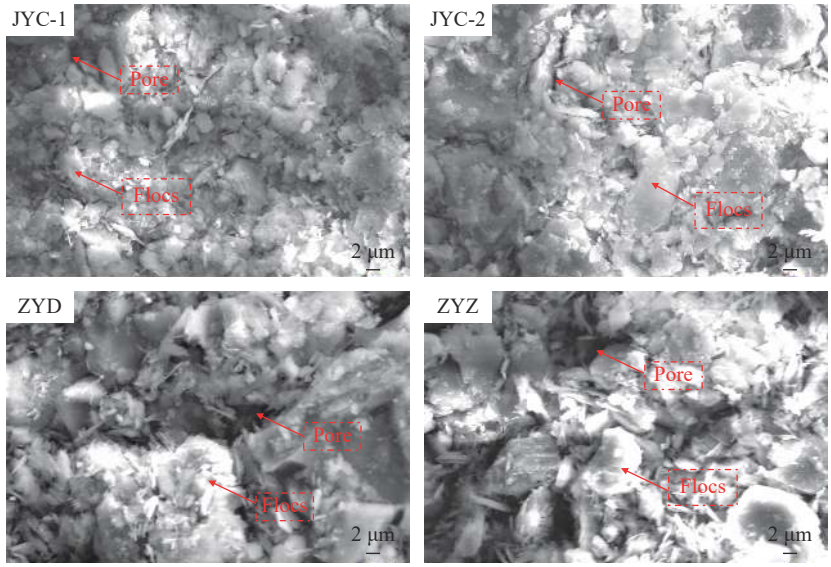

Fig. 6. SEM images of tailings flocculation with different flocculants.

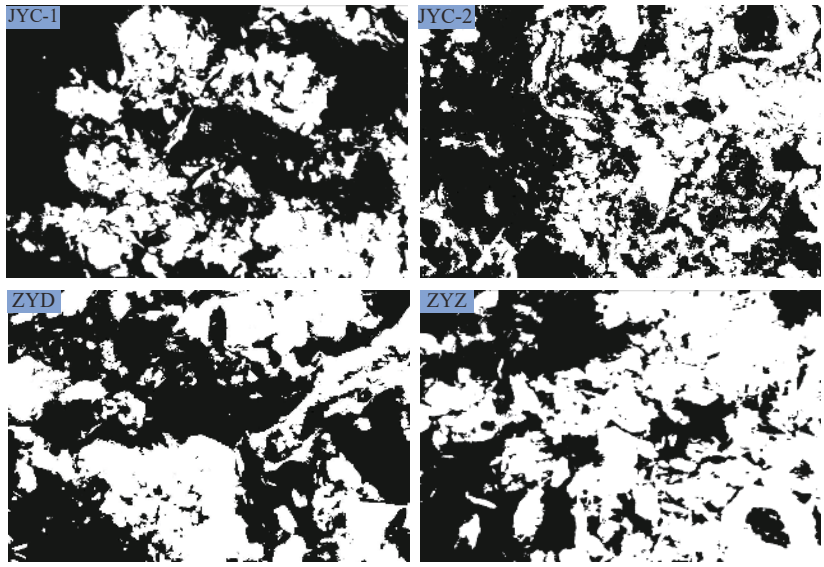

Fig. 7. Binary images of tailings flocculation with different flocculants.

four flocculant types, and the fractal characteristic curve is shown in Fig. 8. Under the action of Brownian movement and turbulence, unclassified tailings flocs make the tailings particles collide and combine with the flocculant. The successful fitting of the fractal characteristic curve indicates that unclassified tailings flocs are an irregular cluster with fractal characteristics. After different flocculants are added to the tailings, flocculation settlement occurs. The fractal dimension is used as a quantitative control parameter to characterize the flocculation structure and evaluate the flocculation effect. The fractal dimensions are 1.816, 1.827, 1.832, and 1.825.

The relationship between flocculant type and fractal di-

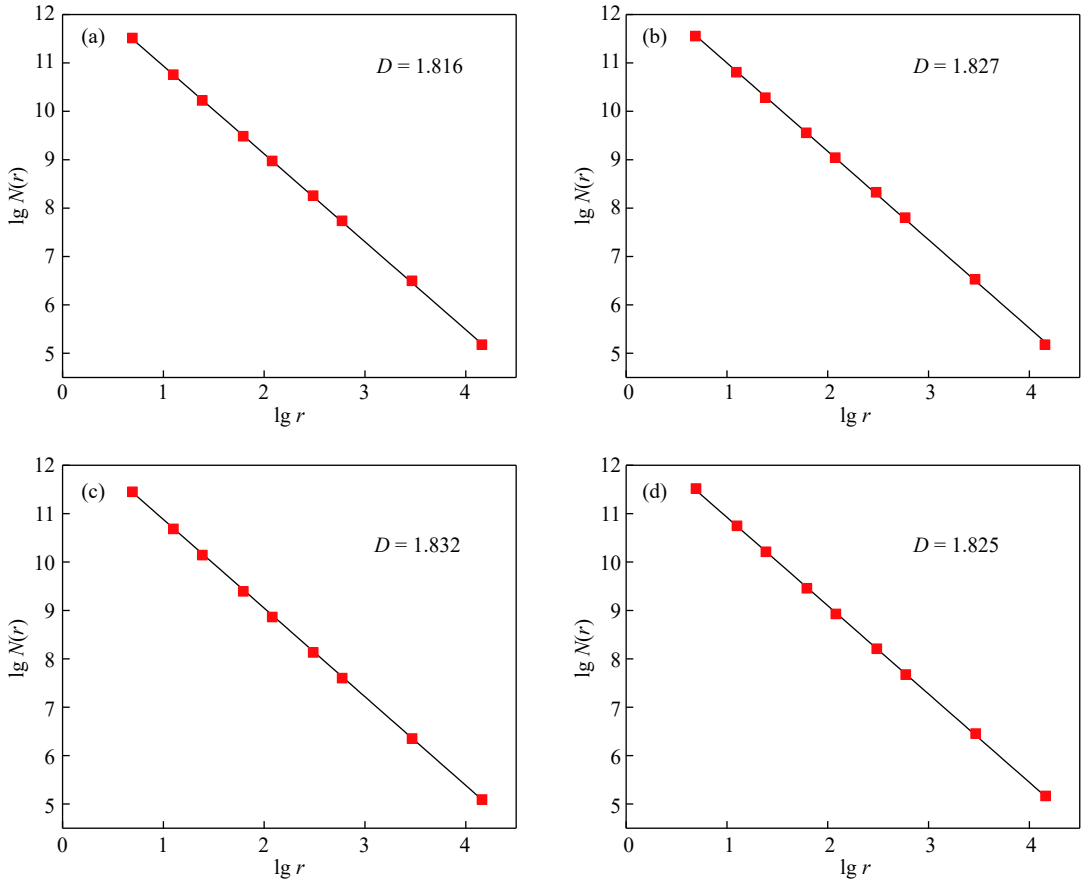

Fig. 8. Fractal characteristic curves of flocs: (a) JYC-1; (b) JYC-2; (c) ZYZ; (d) ZYD.

mension is plotted in Fig. 9. The fractal dimension of the flocculation structure of ZYZ is the largest among the flocculant samples. This result indicates that the tighter the floc is, the larger the molecular weight of the flocculant. This characteristic is beneficial to the rapid settlement of water. The smaller the distance between the particles inside the floc is, the greater the difference between the density of the floc and the density of the liquid and the greater the settling velocity. Therefore, the flocculation effect is good. According to the fractal theory, the ZYZ flocculant has the best flocculation and settling effects on gold mine tailings. The order of the four flocculant types for gold mine tailings is ZYZ > JYC-2 > ZYD > JYC-1.

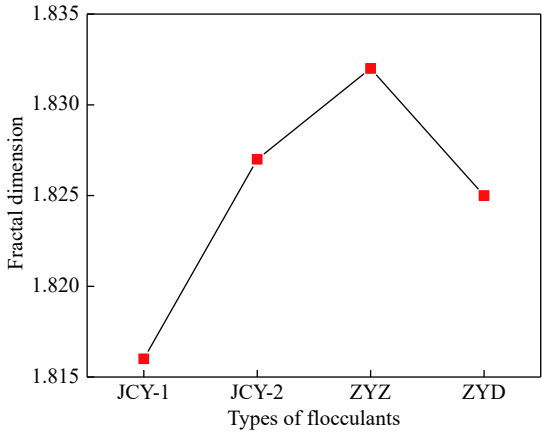

Fig. 9. Relationship between flocculant type and fractal dimension.

3.2. Spatial morphology analysis of ZYZ flocculant tailings floc

The flocs from the top, middle, and bottom of the ZYZ flocculant are magnified 5000× by SEM. The SEM image is in grayscale. However, the human eye has limited ability to distinguish grayscale levels and its nuances. According to the Weber–Fechner law, the visual resolution of the human eye is significantly affected by the color vision and visual contrast of the image. Therefore, the contrast of the grayscale SEM image can be expanded, and the color category can be increased to enhance the visual difference of the combined SEM image, thereby highlighting the subtle differences.

Pseudo-color enhancement technology is used to disguise grayscale or black-and-white images as color maps. In this process, each grayscale of the image is converted into a point in the color space according to a certain functional relationship, so that the image has different grayscales. Thus, the human eye can easily recognize different colors and the purpose of image enhancement can be achieved.

Fig. 10 shows the SEM images after processing with the pseudo-color enhancement technology. The grayscale values are sequentially defined as red, yellow, green, white, cyan, blue, and others. Some areas are extracted, and the grayscale value is converted into a three-dimensional figure.

Figs. 10(a)−10(c) show the SEM images of different settlement heights of the sampling locations illustrated in Fig. 3. At location 1 (top), the size of the floc is large, and most of the flocs greater than 20 μm have a concentrated distribution. Large pores greater than 10 μm are also present. At location 2 (middle), the floc size is evenly distributed between 15 and 20 μm, and the pore size is significantly reduced. At location 3 (bottom), the floc size is less than 15 μm, and small flocs exist. Small pores increase in size and are evenly distributed around the flocs. As the settlement height decreases, the size of the tailings floc decreases. During the flocculation and settling of tailings flocs, large flocs settle and become dehydrated into small flocs.

3.3. Grayscale characteristic analysis of the tailings floc in ZYZ

The grayscale value refers to the dark range of the image, where the white and black values are 255 and 0, respectively. In the original SEM image, black corresponds to the pores between flocculation structures, and the floc entities show different degrees of white. The grayscale characteristics of the tailings floc in ZYZ are analyzed as follows. The grayscale analysis is performed for the same position of the SEM images of different locations of the flocculation settlement (Fig. 11).

Figs. 11(a)−11(c) are extracted from the top, middle, and bottom of the ZYZ flocculant tailings settlement, respectively. The curve illustrated in the figure shows the distribution of the grayscale value at the horizontal red line. The grayscale value can intuitively indicate the difference between pores and solids. Fig. 11(a) illustrates that the top grayscale value of the floc is greater than 250. Only one pore has a grayscale value of less than 50. The average grayscale value is 144. Fig. 11(b) shows the conditions in the middle part. The grayscale value of the floc is preferably approximately 200, and three pores have a grayscale value of less than 50. The average grayscale value of the middle part is 109. In Fig. 11(c), the grayscale value at the bottom is significantly less than 200, and the grayscale value of most pores is less than 50. The average grayscale value is 103. The average grayscale value of the floc decreases with the decrease in settlement height (Fig. 11). This finding indicates that the tailings flocs at the top have a high water content; thus, the floc appears bright white. During flocculation settlement, the internal water of the flocs is continuously exported, and the color of the flocs gradually darkens. Therefore, the grayscale value gradually decreases.

3.4. Microscopic characterization of the pore structure of ZYZ flocculant tailings floc

3.4.1. Three-dimensional pore model

Three-dimensional reconstruction is performed by im-

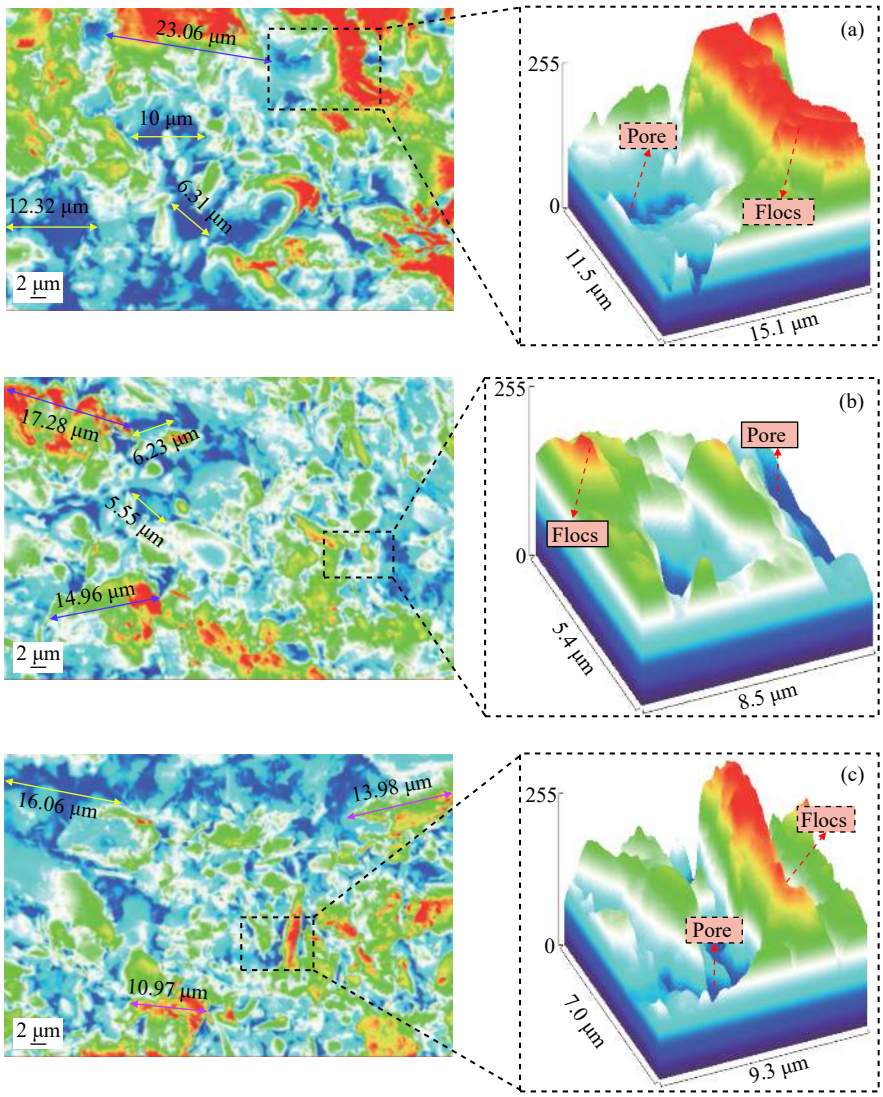

Fig. 10. SEM images of tailings flocculation of the ZYZ flocculant: (a) location 1; (b) location 2; (c) location 3.

porting the μCT data files to be reconstructed, constructing a three-dimensional data set, and adjusting the reconstruction parameters. The reconstructed image is shown in Fig. 12. The blue part denotes the pores, and the red part denotes the floc entities. The pores and floc entities are separated through threshold segmentation. The pores are extracted separately to establish a three-dimensional pore model, and the height of the reconstructed model is 10 mm.

3.4.2. Characteristics of the spatial distribution of pores in tailings floc

Pore slices with settlement heights of 10, 8, 6, 4, 2, and 0 mm are taken according to the reconstructed structure to analyze the effect of sample settlement height on pore distribution (Fig. 13). The pore distribution of the sample shows different characteristics as the settlement height varies. The pores at the bottom of the sample (0 mm) are loose. As the settlement height increases, the pores of the sample gradually increase. The settlement height of the sample remarkably affects the pores. The interpenetration between the pores at the bottom of the sample is relatively poor in a scattered distribution, and most of them are independent pores. At the top of the sample, the pores are distributed on a flat surface, and the penetration between them is relatively good.

3.4.3. Quantitative analysis of the settlement height and the quantity and size of pores

In the study of the thickening mechanism of unclassified tailings, the floc size affects the settling rate, and the addition of flocculant improves the efficiency of solid–liquid separation. The microscopic structure is the main reason that unclassified tailings become dense. Therefore, ZYZ is examined through μCT scanning to obtain the slice image data. The relationship between the settlement height and the number and size of pores is determined by extracting the pore data of each layer.

Fig. 14 shows the relationship between number of pores and settlement height. The number of pores gradually in-

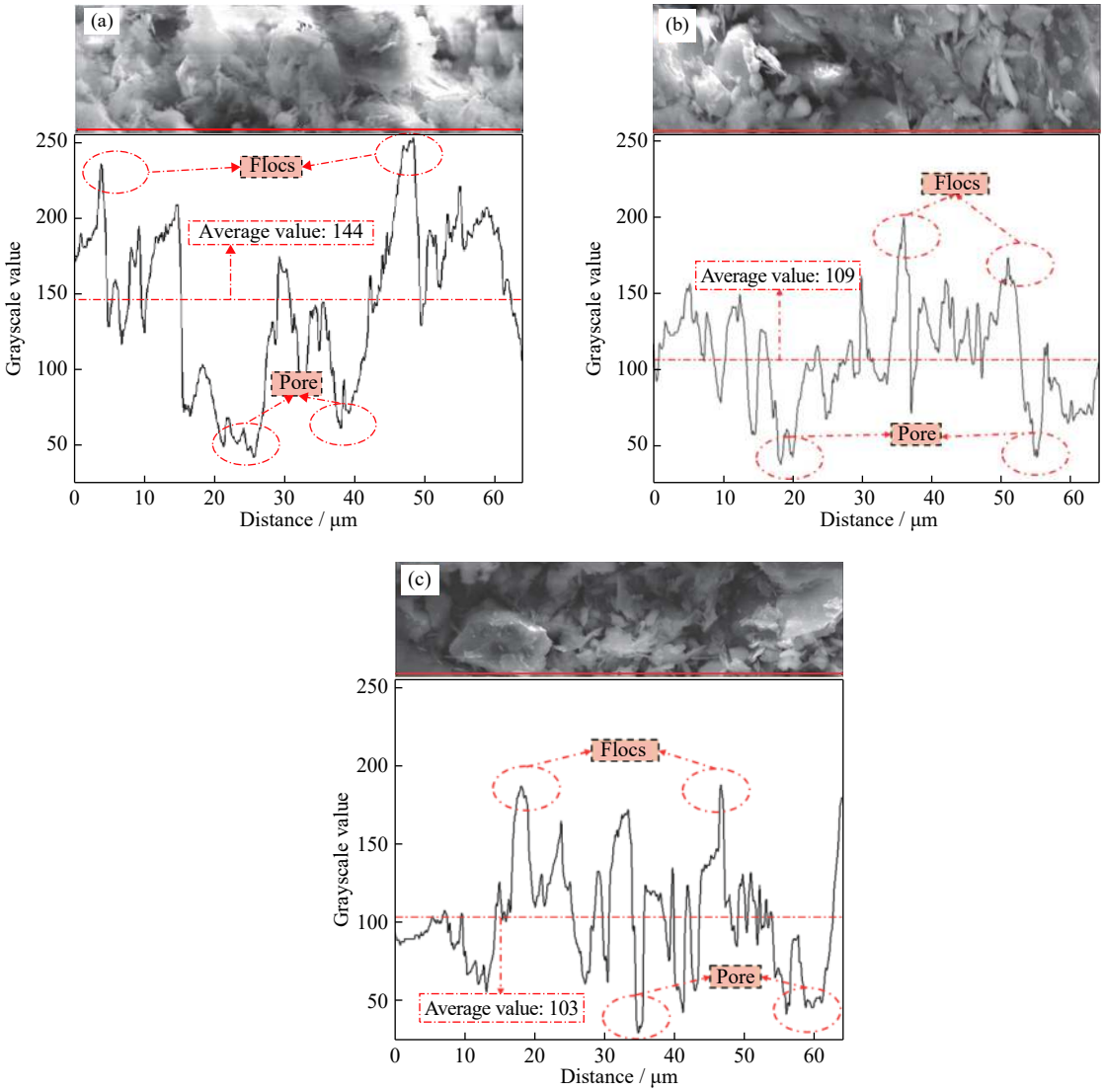

Fig. 11. Grayscale value characteristic curve of flocs: (a) location 1; (b) location 2; (c) location 3.

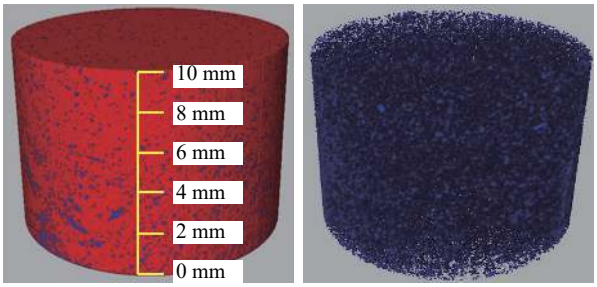

Fig. 12. Three-dimensional pore model of the ZYZ flocculant tailings floc.

creases with the increase in settlement height. Thus, the number of pores is exponentially related to the settlement height. The correlation coefficient $R^2 = 0.987$ indicates that the exponential function has a high correlation, and the exponential equation relation is $y = e^{a+bx+cx^2}$, where a, b, and c are constants ($a = 7.222$, $b = -0.013$, $c = 0.009$). As flocculation settlement continues to occur, the tailings flocs are deposited at the bottom; thus, the number of pores is gradually reduced. Approximately 2700 and 1400 pores are detected at the top and bottom, respectively.

Fig. 15 shows the relationship between pore size and settlement height. The difference is approximately 4 μm, indicating that the overall change in pore size is nonsignificant. The size of the top pore of the floc is small, indicating that the size of the top floc is large. As the settlement height increases, the overall trend of the size of the floc initially increases and subsequently decreases. After nonlinear fitting is performed, $R^2 = 0.848$, and the degree of fitting is high. The pore size and settlement height satisfy the following nonlinear formula: $y = y_0 + (A/w) \times \sqrt{x_c/x} \times \text{Bessel\_il}\left(2\sqrt{x_c/x}/w\right) \times e^{((-x_c-x)/w)}$, where $y_0 = 10.872$, $x_c = 7.407$, $w = 2.552$, $A = 121.129$, and Bessel_il is the Bessel function.

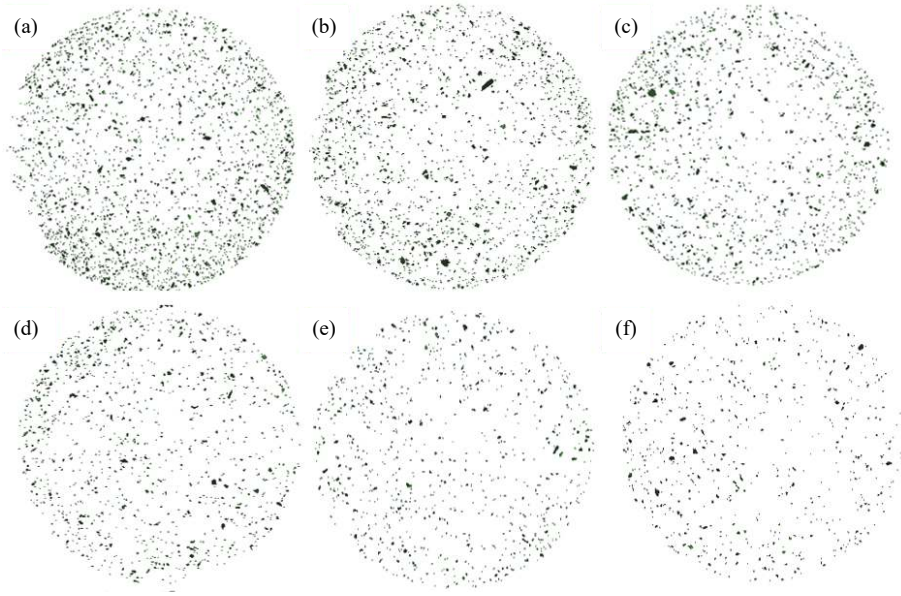

Fig. 13. Microscopic characteristics of pores at different heights: (a) Z = 10 mm; (b) Z = 8 mm; (c) Z = 6 mm; (d) Z = 4 mm; (e) Z = 2 mm; (f) Z = 0 mm.

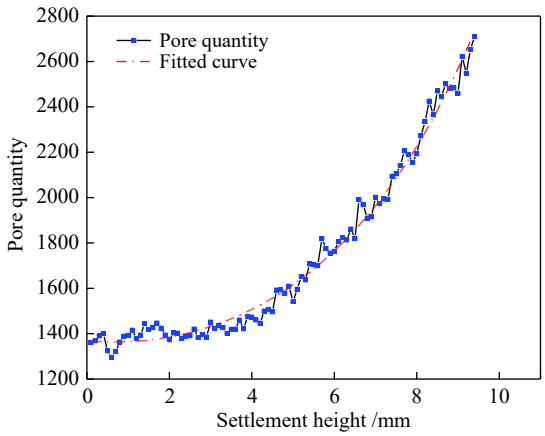

Fig. 14. Relationship between settlement height and pore quantity.

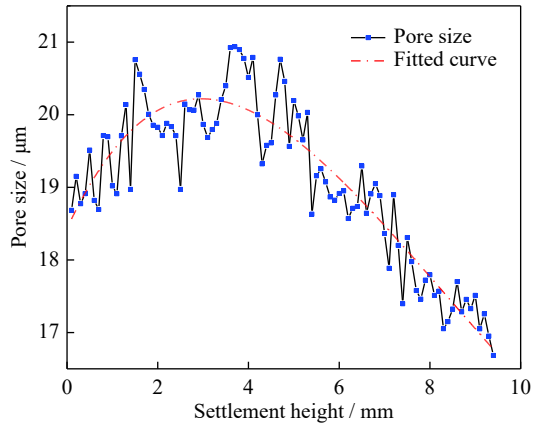

Fig. 15. Relationship between settlement height and pore size.

4. Conclusions

Through a series of indoor experiments, namely, physical property experiments, laser particle size analysis, SEM, μCT scanning, fractal analysis, and three-dimensional reconstruction of the obtained data, the following conclusions are drawn.

(1) The fractal analysis of the SEM image indicates that the fractal dimension of the flocculation structure of ZYZ is the largest among the flocculant samples. This result indicates that the more compact the floc is, the greater the difference between floc density and liquid density, the greater the settling velocity, and the better the flocculation effect. The flocculation effect of the four flocculant types has the following trend: ZYZ > JYC-2 > ZYD > JYC-1.

(2) The spatial shape of the floc is analyzed by rendering the SEM image into color through the pseudo-color enhancement technology. For the tailings floc in the ZYZ flocculant, the floc size decreases continuously, and the average gray-scale value of the floc decreases with the decrease in settlement height.

(3) A three-dimensional pore model of the sample is constructed. The results indicate that settlement height remarkably affects pores. The interpenetration between the pores at the bottom of the sample is relatively poor in a scattered distribution, whereas the interpenetration between the pores at the top of the sample is better.

(4) As settlement height increases, the number of pores gradually increases. The number of pores is exponentially related to the settlement height. The difference in pore size is approximately 4 μm, indicating that the overall pore size is not considerably changed. As the settlement height increases, the pore size initially increases and subsequently decreases.

Acknowledgements

This work was financially supported by the National Natural Science Foundation of China (Nos. 51974012 and 51804017), the National Key Research and Development Program of China (No. 2018YFC0604602), the Fundamental Research Funds for the Central Universities, China (No. FRF-BD-19-005A), and the Opening Fund of State Key Laboratory of Nonlinear Mechanics (No. LNM202009).

References

[1] X. Zhao, A. Fourie, and C.C. Qi, An analytical solution for evaluating the safety of an exposed face in a paste backfill stope incorporating the arching phenomenon, *Int. J. Miner. Metall. Mater.*, 26(2019), No. 10, p. 1206.

[2] Y.Y. Tan, X. Yu, D. Elmo, L.H. Xu, and W.D. Song, Experimental study on dynamic mechanical property of cemented tailings backfill under SHPB impact loading, *Int. J. Miner. Metall. Mater.*, 26(2019), No. 4, p. 404.

[3] M.F. Cai, D.L. Xue, and F.H. Ren, Current status and development strategy of metal mines, *Chin. J. Eng.*, 41(2019), No. 4, p. 417.

[4] S. Cao and W.D. Song, Effect of filling interval time on the mechanical strength and ultrasonic properties of cemented coarse tailing backfill, *Int. J. Miner. Process.*, 166(2017), p. 62.

[5] H.Y. Wang, *Research on the Key Technologies of Mud Making Andtailing Releasing of Vertical Sand Tank in Fankoulead-Zinc Mine* [Dissertation], Central South University, Hunan, 2009.

[6] K. Tudu, S. Pal, and N.R. Mandre, Comparison of selective flocculation of low grade goethitic iron ore fines using natural and synthetic polymers and a graft copolymer, *Int. J. Miner. Metall. Mater.*, 25(2018), No. 5, p. 498.

[7] S. Wang, X.P. Song, X.J. Wang, Q.S. Chen, J.C. Qin, and Y.X. Ke, Influence of coarse tailings on flocculation settlement, *Int. J. Miner. Metall. Mater.*, 27(2020), No. 8, p. 1065.

[8] C. Cruz, J. Ramos, P. Robles, W.H. Leiva, R.I. Jeldres, and L.A. Cisternas, Partial seawater desalination treatment for improving chalcopyrite floatability and tailing flocculation with clay content, *Miner. Eng.*, 151(2020), art. No. 106307.

[9] D.L. Wang, Q.L. Zhang, Q.S. Chen, C.C. Qi, Y. Feng, and C.C. Xiao, Temperature variation characteristics in flocculation settlement of tailings and its mechanism, *Int. J. Miner. Metall. Mater.*, 27(2020), No. 11, p. 1438.

[10] L. Panda, P.K. Banerjee, S.K. Biswal, R. Venugopal, and N.R. Mandre, Performance evaluation for selectivity of the flocculant on hematite in selective flocculation, *Int. J. Miner. Metall. Mater.*, 20(2013), No. 12, p. 1123.

[11] Y. Wang, A.X. Wu, H.J. Wang, S.Z. Liu, and B. Zhou, Influence mechanism of flocculant dosage on tailings thickening, *J. Univ. Sci. Technol. Beijing*, 35(2013), No. 11, p. 1419.

[12] Y. Yang, A.X. Wu, B. Klein, and H.J. Wang, Effect of primary flocculant type on a two-step flocculation process on iron ore fine tailings under alkaline environment, *Miner. Eng.*, 132(2019), p. 14.

[13] Q.Y. Lu, B. Yan, L. Xie, J. Huang, Y. Liu, and H.B. Zeng, A two-step flocculation process on oil sands tailings treatment using oppositely charged polymer flocculants, *Sci. Total Environ.*, 565(2016), p. 369.

[14] L. Han, D.Q. Gan, Z.Y. Liu, and W.Z. Lv, Experimental study on the flocculation and sedimentation laws of total tailings, *Min. Res. Dev.*, 37(2017), No. 3, p. 39.

[15] Q. Zhou, J.H. Liu, A.X. Wu, H.J. Wang, S.F. Fu, and Y. Gu, Effect and mechanism of synergist on tailings slurry thickening performance, *Chin. J. Eng.*, 41(2019), No. 11, p. 1405.

[16] W.J. Zou, Y.J. Cao, C.B. Sun, and Z.J. Zhang, Mechanism of action of polyacrylamide in selective flocculation flotation of fine coal, *Chin. J. Eng.*, 38(2016), No. 3, p. 299.

[17] M. Ejtemaei, S. Ramli, D. Osborne, and A.V. Nguyen, Synergistic effects of surfactant−flocculant mixtures on ultrafine coal dewatering and their linkage with interfacial chemistry, *J. Cleaner Prod.*, 232(2019), p. 953.

[18] C. Eswaraiah, S.K. Biswal, B.K. Mishra, Settling characteristics of ultrafine iron ore slimes, *Int. J. Miner. Metall. Mater.*, 19(2012), No. 2, p. 95.

[19] A.X. Wu, Z.E. Ruan, J.D. Wang, S.H. Yin, and C.M. Ai, Optimizing the flocculation behavior of ultrafine tailings by ultraflocculation, *Chin. J. Eng.*, 41(2019), No. 8, p. 981.

[20] H.Z. Jiao, H.J. Wang, A.X. Wu, X.W. Ji, Q.W. Yan, and X. Li, Rule and mechanism of flocculation sedimentation of unclassified tailings, *J. Univ. Sci. Technol. Beijing*, 32(2010), No. 6, p. 702.

[21] H.Z. Jiao, A.X. Wu, H.J. Wang, X.H. Liu, S.K. Yang, and Y.T. Xiao, Experiment study on the flocculation settlement characteristic of unclassified tailings, *J. Univ. Sci. Technol. Beijing*, 33(2011), No. 12, p. 1437.

[22] R.K. Dwari, S.I. Angadi, and S.K. Tripathy, Studies on flocculation characteristics of chromite's ore process tailing: Effect of flocculants ionicity and molecular mass, *Colloids Surf. A*, 537(2018), p. 467.

[23] J.W. Bian, X.M. Wang, and C.C. Xiao, Experimental study on dynamic flocculating sedimentation of unclassified tailings, *J. Cent. South Univ. Sci. Technol.*, 48(2017), No. 12, p. 3278.

[24] P. Ofori, A.V. Nguyen, B. Firth, C. McNally, and O. Ozdemir, Shear-induced floc structure changes for enhanced dewatering of coal preparation plant tailings, *Chem. Eng. J.*, 172(2011), No. 2-3, p. 914.

[25] G. Many, X. Durrieu de Madron, R. Verney, F. Bourrin, P.R. Renosh, F. Jourdin, and A. Gangloff, Geometry, fractal dimension and settling velocity of flocs during flooding conditions in the Rhône ROFI, *Estuarine Coastal Shelf Sci.*, 219(2019), p. 1.

[26] G.R. Quezada, J. Ramos, R.I. Jeldres, P. Robles, and P.G. Toledo, Analysis of the flocculation process of fine tailings particles in saltwater through a population balance model, *Sep. Purif. Technol.*, 237(2020), art. No. 116319.

[27] H.Z. Hou, C.P. Li, S.Y. Wang, and B.H. Yan, Study on the mesostructure of compacted area in total tailings thickening, *Met. Mine*, 2019, No. 3, p. 73.

[28] Y.X. Liu, X.S. Dong, Y.P. Fan, X.M. Ma, and M. Chang, Floc characteristics and sedimentation effected by particle size, *China Powder Sci. Technol.*, 23(2017), No. 5, p. 59.

[29] F.S. Niu, X.L. Zhang, J.X. Zhang, and Z.L. Li, Influence of starch on flocculation characteristics and mechanism of hematite, *Min. Metall. Eng.*, 36(2016), No. 6, p. 30.

[30] C.Y. Xu and P. Dong, A dynamic model for coastal mud flocs with distributed fractal dimension, *J. Coastal Res.*, 33(2017), No. 1, p. 218.

[31] H.Z. Jiao, S.F. Wang, A.X. Wu, Y.M. Wang, and Y.X. Yang, Shear evolution and connected mechanism of pore structure in thickening bed of paste, *J. Cent. South Univ. Sci. Technol.*, 50(2019), No. 5, p. 1173.

[32] G.L. Xue, E. Yilmaz, W.D. Song, and S. Cao, Analysis of internal structure behavior of fiber reinforced cement-tailings

matrix composites through X-ray computed tomography, *Composites Part B*, 175(2019), art. No. 107091.
[33] C.L. Lin, A.R. Videla, Q. Yu, and J.D. Miller, Characterization and analysis of porous, brittle solid structures by X-ray micro computed tomography, *JOM*, 62(2010), No. 12, p. 86.
[34] Y. Wang, C.L. Lin, and J.D. Miller, Improved 3D image segmentation for X-ray tomographic analysis of packed particle beds, *Miner. Eng.*, 83(2015), p. 185.
[35] S. Sharma, C.L. Lin, and J.D. Miller, Multi-scale features including water content of polymer induced kaolinite floc structures, *Miner. Eng.*, 101(2017), p. 20.
[36] W.J. Zhang, R.N. Song, B.D. Cao, X.F. Yang, D.S. Wang, X.M. Fu, and Y. Song, Variations of floc morphology and extracellular organic matters (EOM) in relation to floc filterability under algae flocculation harvesting using polymeric titanium coagulants (PTCs), *Bioresour. Technol.*, 256(2018), p. 350.
[37] J.H. Du, R.A. Pushkarova, and R.S.C. Smart, A cryo-SEM study of aggregate and floc structure changes during clay settling and raking processes, *Int. J. Miner. Process.*, 93(2009), No. 1, p. 66.
[38] A.R. Heath, P.A. Bahri, P.D. Fawell, and J.B. Farrow, Polymer flocculation of calcite: Relating the aggregate size to the settling rate, *AIChE J.*, 52(2006), No. 6, p. 1987.
[39] A. Costine, J. Cox, S. Travaglini, A. Lubansky, P. Fawell, and H. Misslitz, Variations in the molecular weight response of anionic polyacrylamides under different flocculation conditions, *Chem. Eng. Sci.*, 176(2018), p. 127.
[40] M. Jeldres, E.C. Piceros, N. Toro, D. Torres, P. Robles, W.H. Leiva, and R.I. Jeldres, Copper tailing flocculation in seawater: Relating the yield stress with fractal aggregates at varied mixing conditions, *Metals*, 9(2019), No. 12, art. No. 1295.
[41] M.A. Ramírez-Ortegón, E.A. Duéñez-Guzmán, R. Rojas, and E. Cuevas, Unsupervised measures for parameter selection of binarization algorithms, *Pattern Recognit.*, 44(2011), No. 3, p. 491.